Journal of Marine Systems 174 (2017) 25–39

Contents lists available at ScienceDirect

Journal of Marine Systems

journal homepage: www.elsevier.com/locate/jmarsys

Recirculation of the Canary Current in fall 2014

Alonso Hernández-Guerra [a,*], Elisabet Espino-Falcón [a], Pedro Vélez-Belchí [b], M. Dolores Pérez-Hernández [a,c], Antonio Martínez-Marrero [a], Luis Cana [a]

[a] Instituto de Oceanografía y Cambio Global, IOCAG, Universidad de Las Palmas de Gran Canaria, ULPGC, Canary Islands, Spain
[b] Centro Oceanográfico de Canarias, Instituto Español de Oceanografía, Santa Cruz de Tenerife, Canary Islands, Spain
[c] Woods Hole Oceanographic Institution, Woods Hole, MA, United States

ARTICLE INFO

Article history:
Received 28 October 2016
Received in revised form 3 April 2017
Accepted 8 April 2017
Available online 13 May 2017

Keywords:
Canary Current
Recirculation of the Canary Current
Intermediate Poleward Undercurrent
Lanzarote Passage

ABSTRACT

Hydrographic measurements together with Ship mounted Acoustic Doppler Current Profilers and Lowered Acoustic Doppler Current Profilers (LADCP) obtained in October 2014 are used to describe water masses, geostrophic circulation and mass transport of the Canary Current System, as the Eastern Boundary of the North Atlantic Subtropical Gyre. Geostrophic velocities are adjusted to velocities from LADCP data to estimate an initial velocity at the reference layer. The adjustment results in a northward circulation at the thermocline layers over the African slope from an initial convergent flow. Final reference velocities and consequently absolute circulation are estimated from an inverse box model applied to an ocean divided into 13 neutral density layers. This allows us to evaluate mass fluxes consistent with the thermal wind equation and mass conservation. Ekman transport is estimated from the wind data derived from the Weather Research and Forecasting model. Ekman transport is added to the first layer and adjusted with the inverse model. The Canary Current located west of Lanzarote Island transports to the south a mass of -1.5 ± 0.7 Sv ($1\ \text{Sv} = 10^6\ \text{m}^3\ \text{s}^{-1} \approx 10^9\ \text{kg}\ \text{s}^{-1}$) of North Atlantic Central Water at the surface and thermocline layers (~0–700 m). In fall 2014, hydrographic data shows that the Canary Current in the thermocline (below at about 80 m depth to ~700 m) recirculates to the north over the African slope and flows through the Lanzarote Passage. At intermediate layers (~700–1400 m), the Intermediate Poleward Undercurrent transports northward a relatively fresh Antarctic Intermediate Water in the range of 0.8 $\pm$ 0.4 Sv through the Lanzarote Passage and west of Lanzarote Island beneath the recirculation of the Canary Current.

1. Introduction

Subtropical gyres are comprised of intense western boundary currents flowing poleward and slower interior ocean currents flowing equatorward. The southward flowing Canary Current (CC) is the eastern boundary current of the North Atlantic Subtropical Gyre. Historical hydrographic data were used for the first studies of the CC (Stramma, 1984; Stramma and Isemer, 1988; Stramma and Müller, 1989; Stramma and Siedler, 1988). These authors estimated the seasonal variability of the geostrophic transport in the Eastern Subtropical North Atlantic, observing a change in the gyre's structure: In summer, the Canary Current approaches the African upwelling system and the Azores and North Equatorial Currents move south and north, respectively. In the second half of the 90's under the CANIGO project (Parrilla, 2002), specific cruises were carried out in the eastern branch of the CC that flows through the Lanzarote Passage (LP) (Fig. 1). Hernández-Guerra et al. (2001, 2002) were the first to describe the northward flow at the thermocline and intermediate layers in fall in the LP. This pattern of circulation through the LP was later confirmed with current-meter data (Fraile-Nuez et al., 2010; Hernández-Guerra et al., 2003; Pérez-Hernández et al., 2015) and various hydrographic cruises (Hernández-Guerra et al., 2005; Machín et al., 2006; Pérez-Hernández et al., 2013) also extending to the west of the LP sampling the main path of the CC.

Pelegrí et al. (2005) suggested that the dynamical processes explaining the CC are different than those that explain the flow through the LP. The dynamic of the CC is presumably explained by the curl of the wind stress through the Sverdrup theory (Fraile-Nuez and Hernández-Guerra, 2006; Mason et al., 2011; Roemmich and Wunsch, 1985). On the other hand, the circulation through the LP is apparently linked to the upwelling dynamics off northwest Africa and is named the Canary Upwelling Current (CUC) following Laiz et al. (2012) and Pelegrí et al. (2006). The persistence and strength of the northwest Africa upwelling is linked to the Azores High that provides the Trade Winds flowing along the African coast (Wooster et al., 1976). The Azores High presents a seasonal variability with its northernmost position in summer. The upwelling favorable winds in the Canary Islands are

* Corresponding author.
E-mail address: alonso.hernandez@ulpgc.es (A. Hernández-Guerra).

http://dx.doi.org/10.1016/j.jmarsys.2017.04.002
0924-7963/

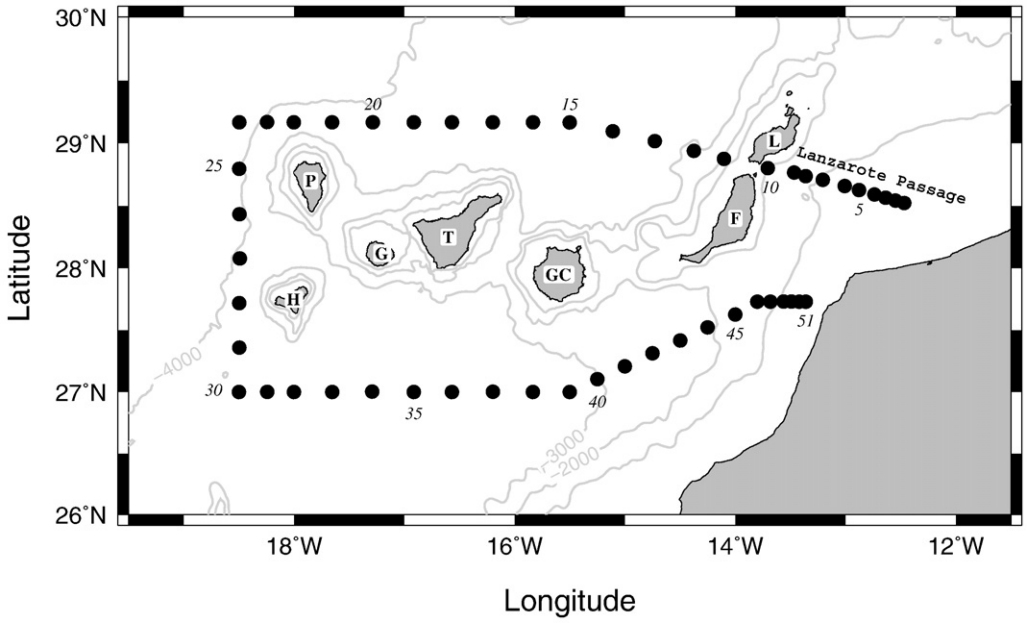

Fig. 1. Studied region. Dots correspond to the geographical location of the stations in Raprocan 1410 carried out in October 2014 (Tel et al., 2016). P stands for La Palma, H for El Hierro, G for La Gomera, T for Tenerife, GC for Gran Canaria, F for Fuerteventura and L for Lanzarote. The Lanzarote Passage between the Lanzarote Island and the African coast is shown. Bathymetry in m (Smith, 1997).

developed during the whole year but are stronger and more persistent during summer (Benazzouz et al., 2014; Hernández-Guerra and Nykjaer, 1997; Marcello et al., 2011; Nykjaer and Van Camp, 1994).

Machín et al. (2006) used four cruises carried out in 1997 and 1998 to estimate the average circulation of the CC and CUC and their seasonal behavior. The mean CC flows to the south with a transport of -2.1 ± 0.9 Sv

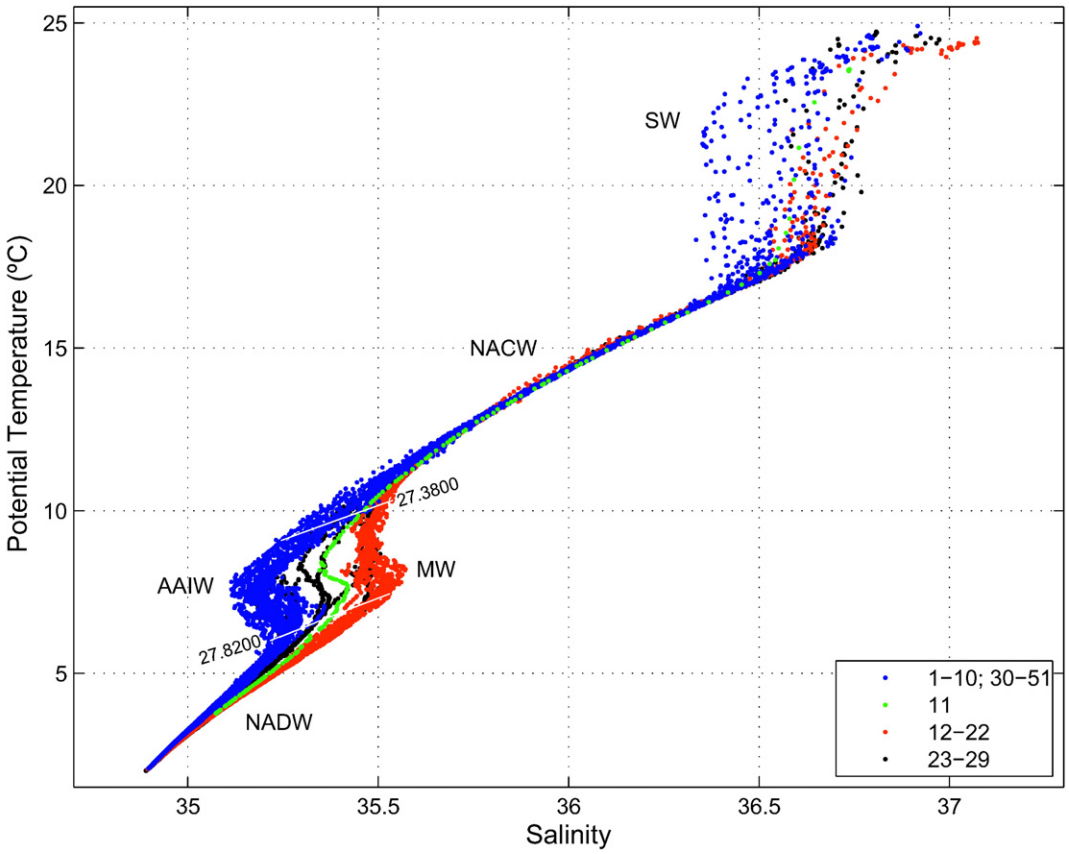

Fig. 2. Potential temperature/salinity diagram for all stations. The main water masses are shown with their corresponding acronyms. Blue dots correspond to stations 1–10 and 30–51; green dots correspond to station 11; red dots correspond to stations 12–22 and black dots correspond to stations 23–29. Plotted white lines are the isoneutrals $\gamma^n = 27.38$ and 27.82 kg/m^3 which roughly divide the water column into surface-central, intermediate and deep waters.

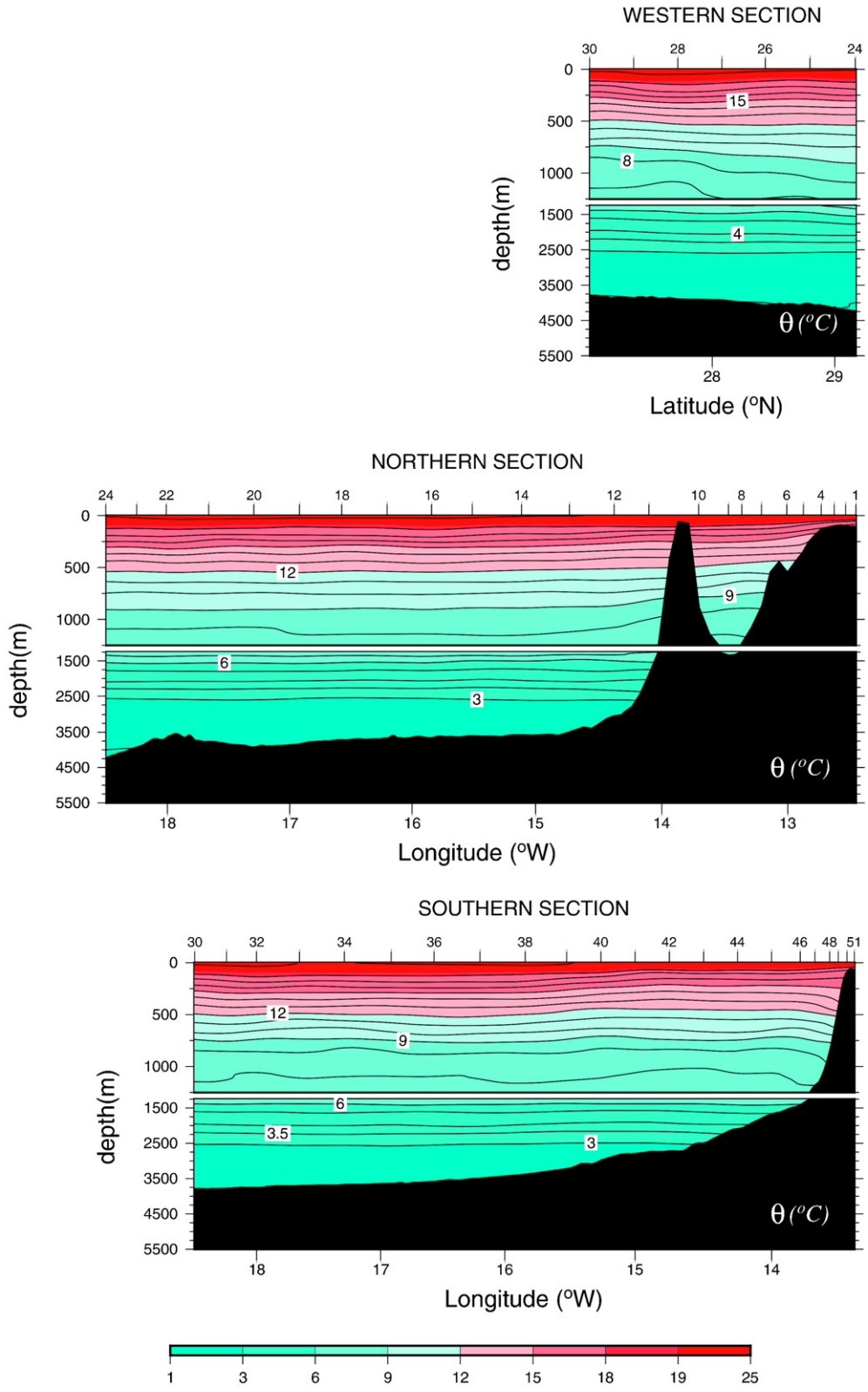

Fig. 3. Vertical sections of potential temperature (in °C) for the western section (upper subplot), northern section (middle subplot) and southern section (lower subplot). Note that x axis represents latitude for the western section and longitude for northern and southern sections.

carrying North Atlantic Central Water (NACW) in the thermocline layers (~0–700 m depth) (hereafter negative transports refer to southward and westward flows). The mean CC flows throughout the entire Canary Archipelago. The CC presents a seasonal variability with a change in intensity and location. The CC transports -2.8 ± 0.8 Sv southward through the western Canary Islands in spring, and -2.9 ± 0.8 Sv southward through the whole Canary Archipelago in summer. In fall and winter, the CC almost disappears through the Canary Islands. During these seasons, the CC presumably flows west of the Canary Islands as described in Pérez-Hernández et al. (2013). They applied an

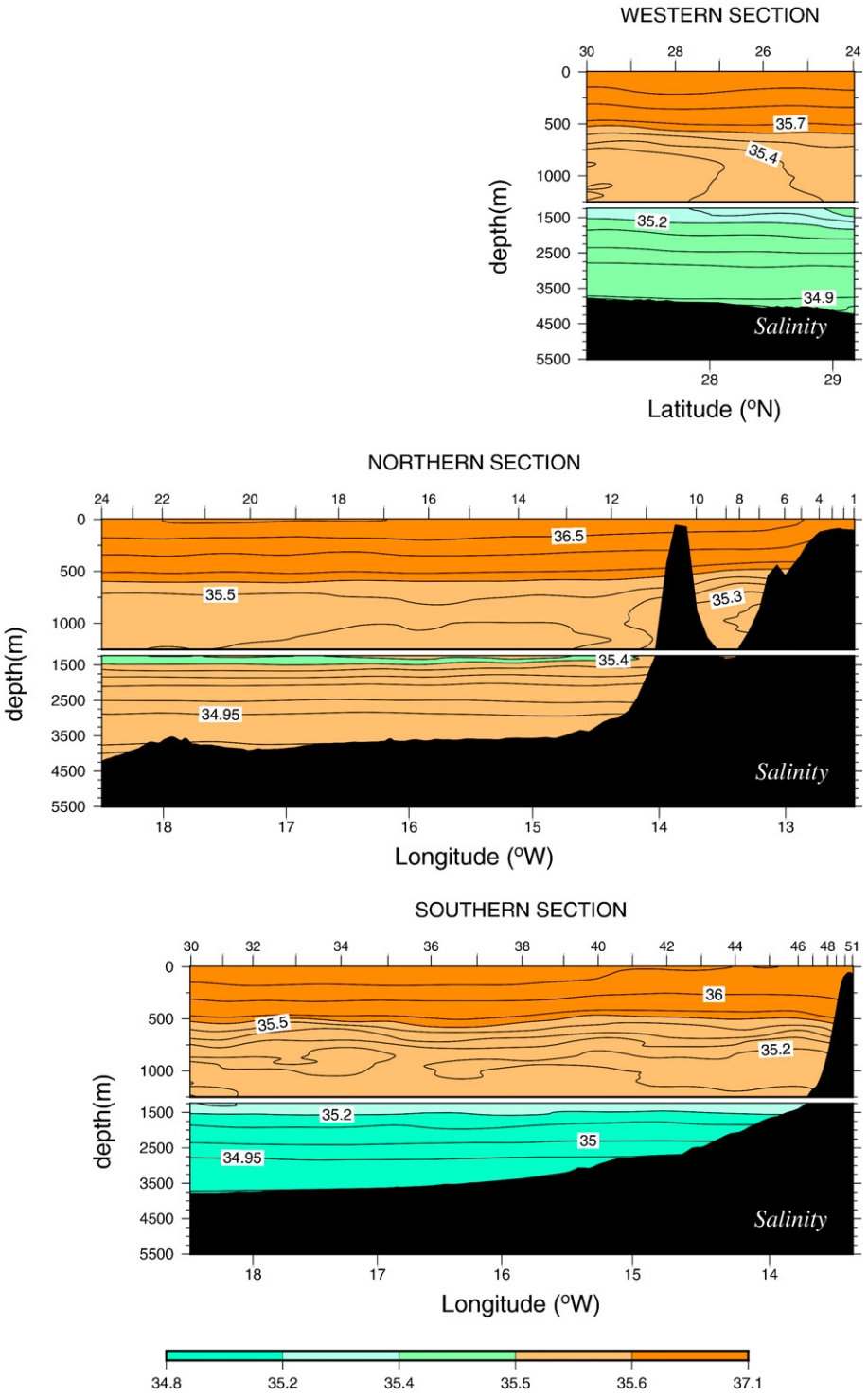

Fig. 4. Vertical sections of salinity for the western section (upper subplot), northern section (middle subplot) and southern section (lower subplot). Note that x axis represents latitude for the western section and longitude for northern and southern sections.

inverse model to a cruise carried out in fall 2009 that extended west of the islands. They observed a strong CC transporting -6.2 ± 0.6 Sv south, west of the Canary Islands. This high transport is presumably due to the merging of the CC transport and a second branch from the Azores Current (Comas-Rodriguez et al., 2011). This pattern of the seasonal variability of the CC has been also reproduced in the frame of a Regional Oceanic Modeling System (ROMS) (Mason et al., 2011). They determined that the variability of the CC is mediated by the westward passages of baroclinic Rossby waves generated by the nearshore wind stress curl variability.

The average transport of the CUC is -0.6 ± 0.1 Sv to the south with small seasonal variability (in the range 0.7–1.2 Sv to the south) except in fall where a northward circulation of 1.8 ± 0.1 Sv is present (Machín et al., 2006). The northward transport of the CUC in fall was previously suggested by Stramma and Isemer (1988) and Stramma and Siedler (1988) south of the Canary Islands from historical data. Mason et al. (2012) also describe the northward circulation through the LP from the stream functions computed in the frame of a 7.5 km ROMS model. This relatively intense flow reversal was also found by Laiz et al. (2012) in November over several years. They suggested that the flow

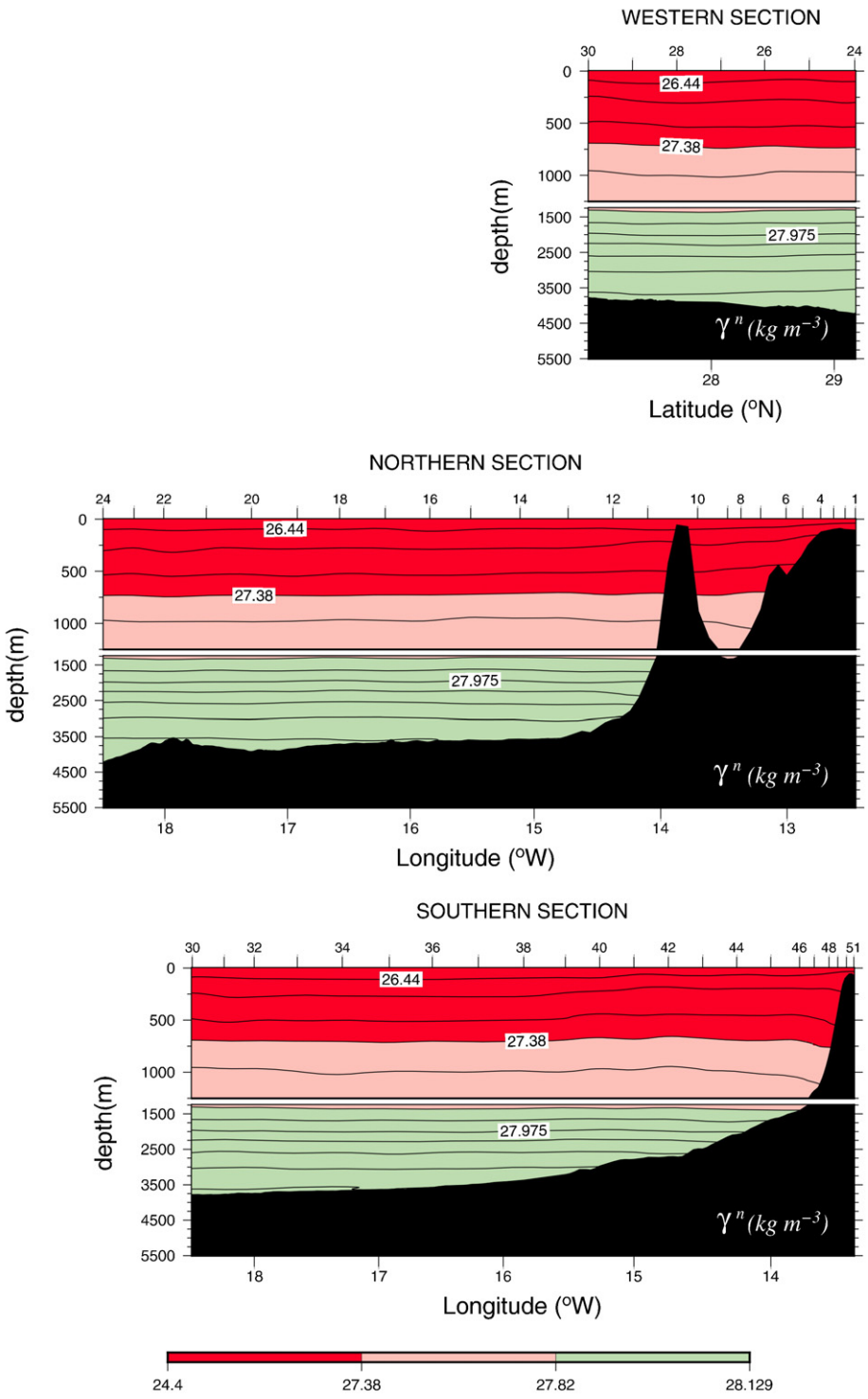

Fig. 5. Vertical sections of Neutral densities γ^n (kg/m^3) for the western section (upper subplot), northern section (middle subplot) and southern section (lower subplot). Note that x axis represents latitude for the western section and longitude for northern and southern sections. Neutral densities γ^n defined by (Ganachaud, 1999) for the North Atlantic Ocean are represented, dividing the ocean closed volume into 13 layers. Surface and thermocline layers correspond to $\gamma^n < 27.38$ kg/m^3 (red); intermediate layers to $27.38 < \gamma^n < 27.82$ kg/m^3 (pink) and deep layers $\gamma^n > 27.82$ kg/m^3 (green).

reversal is probably the result of a late fall intensification of the CUC north of the Canary Islands followed by instabilities and offshore flow diversion. This would lead to the formation of a large cyclonic circulation that can be extended around the islands and a poleward flow thorough the LP as previously speculated by Pelegrí et al. (2005).

At intermediate layers (~700–1400 m), two water masses are commonly found in the Canary Islands area, the Mediterranean Water (MW) and the Antarctic Intermediate Water (AAIW) and they are easily detected by their respective salinity signatures (Hernández-Guerra et al., 2001, 2003). Through the LP, a remarkable content of AAIW is observed due to the northward flow of the Intermediate Poleward Undercurrent (IPUC) (Pérez-Hernández et al., 2015). The IPUC transports AAIW meridionally along the African slope. This water mass expands northward during fall as a core, propagating and stretching progressively along the 27.5 kg/m^3 isoneutral with contributions that reach to 32.5°N (Machín and Pelegrí, 2009; Machín et al., 2010). This poleward

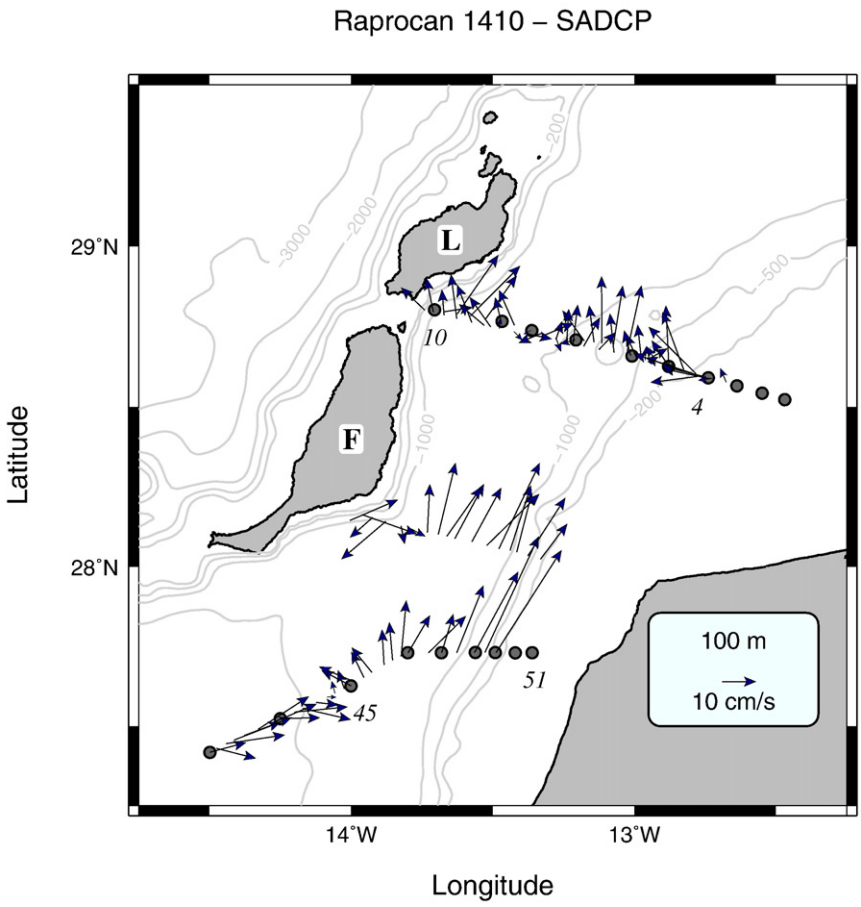

Fig. 6. Velocity at 100 m depth from a SADCP. L stands for Lanzarote island and F for Fuerteventura island.

transport of AAIW during fall is also observed and compared to the CANIGO model in Knoll et al. (2002).

As outlined, the previous studies have measured a southward CC and a northward flow through the LP in fall. The main purpose of this study is to establish the circulation pattern in the Canary Basin in fall 2014 and to estimate from hydrographic data that the northward flow through the LP is a recirculation of the CC. To pursue this objective, an inverse box model is carried out together with water masses determination. The study is presented in the following outlines: Data and methods are presented in Section 2; Section 3 describes the water masses in the region using potential temperature/salinity diagram and vertical sections of potential temperature, salinity and neutral density; in Section 4, a description of the flow over the African slope and through the LP is carried out; in Section 5, the initial geostrophic velocity and LADCP velocity data are compared and geostrophic mass transport estimations are presented; Sections 6 and 7 describe the inverse model used and present the final geostrophic mass transport, respectively. Finally, a discussion and conclusions are provided in Section 8.

2. Data and methods

The data corresponds to a cruise that took place on board of the R/V Ángeles Alvariño in fall 2014 (from 13 to 23 October), a season characterized by relatively weak Trade Winds. The Ekman transport was 10^{-2} Sv in the north and west transect, and $2 \cdot 10^{-2}$ Sv in the south transect. The cruise consisted of 51 hydrographic stations closing a box as shown in Fig. 1. At each station, conductivity, temperature and pressure were measured with redundant temperature and salinity sensors from a Seabird 911+ CTD together with velocities from Lowered Acoustic Doppler Current Profilers (LADCP) data. Data were acquired at each station from the surface down to 10 m above the sea floor. Distance intervals between stations were approximately 50 km except over the African slope and LP in which stations which were 4–5 km apart. The temperature and pressure sensors were calibrated at the SeaBird laboratory before the cruise. On board salinity calibration was carried out with a Guild-line AUTOSAL model 8400 B salinometer with a precision better than 0.002 for single samples.

Velocity data were acquired from two LADCPs Workhorse consisting in a hybrid system (150 kHz and 300 kHz) attached to the rosette and from a 150 kHz Ship mounted ADCP (SADCP) that reaches down to 200 m depth. The LADCP system was run in a master/slave mode, with the 150 kHz LADCP looking downward (master) and with the 300 kHz LADCP looking upward (slave), using a shared battery pack. The processing of LADCP data contains SADCP data in the shallowest layer. The LADCP were processed according to (Fischer and Visbeck, 1993) and SADCP data were processed with CODAS software (http://currents.soest.hawaii.edu/docs/doc/), which requires conducting a test of the return signal as recommended by (Firing and Ranada, 1995). LADCP and SADCP are based on the doppler effect to estimate directly velocity within the water column. However, these instruments have a high noise level and, consequently, the water transport cannot be directly calculated from them. Thus, LADCP is used to estimate a velocity in the assumed layer of no motion by comparing the LADCP velocity profile with the geostrophic velocity profile as suggested by Comas-Rodríguez et al. (2010).

Wind data are estimated using the Weather Research and Forecasting (WRF) model (version 3.4.1), developed at the National Center for Atmospheric Research. In contrast with climatological models, this model has the advantage of obtaining wind data with increased temporal as well as spatial resolution in order to take into account wind variability during the cruise. A complete description of this model can be found in Skamarock et al. (2008). For our simulations, we set for our

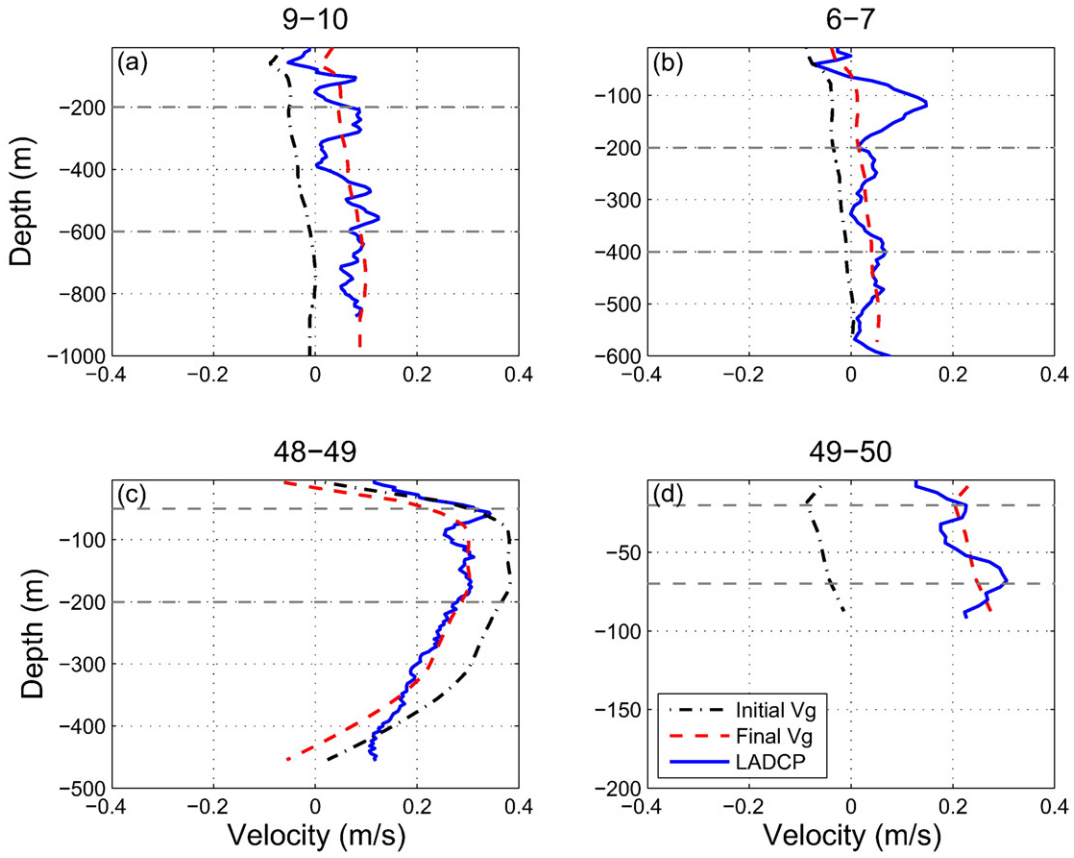

Fig. 7. Comparison between the initial geostrophic velocity profile (black lines) and the LADCP velocity (blue lines). The red lines represent the adjusted initial velocity to LADCP data.

simulations a horizontal grid spacing of 0.125° and 45 terrain-influenced coordinate levels. Spacing between levels ranged from 60 m near the sea floor, about 300 m in the middle and upper troposphere and 400 m towards the top. Finally, data from the operational analysis performed every 6 h at 1° horizontal resolution at the National Center for Environmental Prediction (NCEP final analysis), were used as initial and boundary conditions for the simulations. These data were used to estimate the Ekman transport and introduced in the first layer for each section. Hernández-Guerra and Talley (2016) found no difference in the results after applying the inverse model using a wind averaged over one year prior to the cruise or using wind averaged over the time spanning the cruise. We use the Ekman transport corresponding to the time of the cruise.

3. Water masses

A potential temperature/salinity (θ/S) diagram (Fig. 2) and vertical sections of potential temperature (Fig. 3), salinity (Fig. 4) and neutral density (γ^n) (Fig. 5) are used together to identify water masses and their associated spatial and density/depth distribution. The neutral density of Jackett and McDougall (1997) is used as the density variable throughout this paper. The small range of latitude and longitude ranges of this area allows us to show the isoneutrals in the θ/S diagram.

Surface Water (SW), NACW, AAIW, MW and North Atlantic Deep Water (NADW) are found in the studied area as shown in the θ/S diagram (Fig. 2). The θ/S diagram has been represented indicating the stations where higher content of AAIW (1–10; 30–51), AAIW and MW mixture (11; 23–29) and higher content of MW (12 − 22) is found at intermediate layers. Two selected neutral densities, $\gamma^n = 27.38$ and 27.82 kg/m^3, have been superimposed to roughly divide the water column into surface-central (thermocline layers), intermediate and deep waters as in Hernández-Guerra et al. (2005).

SW-NACW are present in the upper levels (roughly 0–700 m depth) corresponding to the thermocline layer ($\gamma^n < 27.38$ kg/m^3). SW is located above the seasonal thermocline (approximately 80 m) and is characterized by a scattering of potential temperature and salinity values due to the seasonal evaporation and precipitation, as well as to the cold and low-salinity waters advected by upwelling filaments from the upwelling area off northwest Africa (Borges et al., 2004; Nykjaer and Van Camp, 1994; Van Camp et al., 1991). NACW is found below the seasonal thermocline. In every section, the isotherms and isopycnals slopes are quasihorizontal resulting in a small geostrophic velocity shear. Close to the African coast, on both the northern and southern transects, the isotherms (Fig. 3) and isopycnals (Fig. 5) present a little or a slight upward trends in the upper 300 m, while below this depth the slope along the two lines is upwards in the north and downwards in the south. This will result in a convergent flow.

Below the central waters, the intermediate water mass consists of a fresher (<35.3) AAIW and a warmer and saltier (>35.4) MW (Fig. 4). These water masses are found in the range $27.38 < \gamma^n < 27.82$ kg/m^3 (roughly 700–1400 m depth). Spatial distribution of AAIW and MW is well defined: the AAIW signature is stronger in the southern section while the MW signature is stronger in the northern section around stations 11–23. This suggests that a gradual northward/southward contribution of AAIW/MW is present, which can be observed in the western section of Fig. 4. This transition of water masses occurs over a wide latitudinal range. It is noteworthy the high content of AAIW found in the LP with the 35.2 isohaline clearly observed (Fig. 4). This occurrence is also observed in the stations 1–10 in the θ/S diagram. Station 11 located west of the LP still has a contribution of AAIW. In Fig. 5, isoneutrals in the northern and southern sections over the LP and African slope (around stations 6–10 and 45–51, respectively) present negative slopes at intermediate layer, resulting in a northward geostrophic velocity shear of AAIW along the African slope.

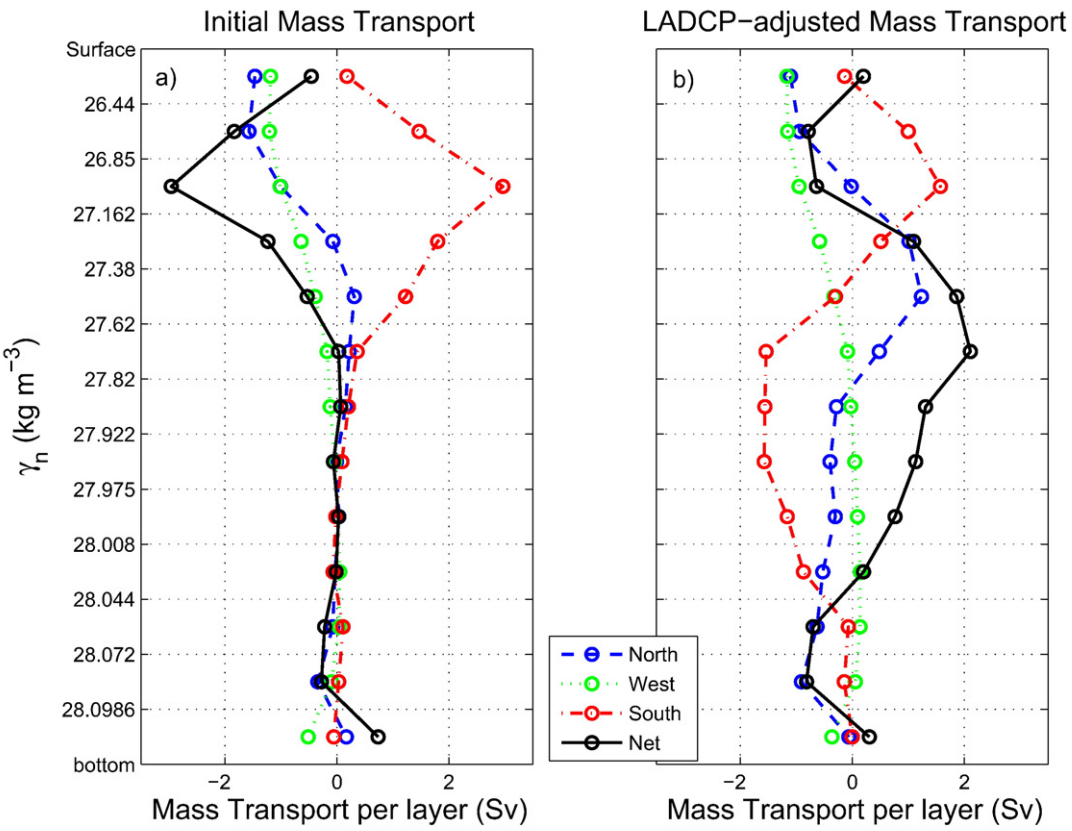

Fig. 8. Integrated geostrophic mass transport per isoneutral layer: north transect (blue), west transect (green) and south transect (red). Imbalance is represented by the black line. a) Initial geostrophic velocity without LADCP adjustment. b) Initial LADCP-adjusted geostrophic velocity. For each transect, positive/negative sign means northward/southward or eastward/westward flow.

Deep layers from approximately 1400 m depth to the sea floor ($\gamma^n > 27.82$ kg/m^3) are composed of NADW (Hernández-Guerra et al., 2005). As shown in Fig. 2–5, NADW appears roughly between $1 < \theta < 6$ °C and $34.8 < S < 35.2$. The slope of the isotherms and isopycnals corresponding to this water mass is approximately flat in every section resulting in a constant geostrophic velocity in these layers. Deep waters will not be further mentioned.

4. The thermocline layers of the Lanzarote Passage and over the African slope

In Fig. 5, isoneutrals in the LP present a shoaling in the thermocline layers, resulting in a negative (southward) geostrophic velocity shear that could be related to the CUC (Pelegrí et al., 2005, 2006). The mass transport through the LP is to the south at a rate of −2.5 Sv with a reference layer at $\gamma^n = 27.38$ kg/m^3. In contrast, isoneutrals of the southern section over the African slope (around stations 45–51) present a deepening, which results in a positive (northward) geostrophic velocity shear. The mass transport over the African slope in the southern transect is 3.1 Sv to the north with a reference layer at $\gamma^n = 27.975$ kg/m^3. This discrepancy in flow direction will be addressed using LADCP data once the velocity at the reference layer is estimated.

Fig. 6 shows the SADCP velocity at about 100 m depth in the eastern sampling area. This figure presents velocity data for the LP, the southern section over the African slope and a middle section. In these three sections northward velocities are observed. The three sections present an overall cross-sectional northward flow at 100 m depth with a mean velocity of 7.5, 10.9 and 12.7 cm s^{-1} in the north, middle and south sections, respectively. Fig. 6 suggests that the main northward flow takes place along the continental slope off the African coast with a maximum cross-sectional northward velocity of 20.0, 27.5 and 34.2 cm s^{-1} in the north, middle and south sections, respectively.

The velocity from LADCP data can be used to estimate the velocity at the reference layer (Joyce et al., 2001). From the thermal wind equation, the density field between two adjacent stations is used to compute the relative geostrophic velocity normal to the vertical plane formed by both stations. The relative geostrophic velocity depends on the selected reference layer. The simplest model would set the reference level as no motion and calculate the geostrophic velocity field referenced to that level. In this study, we have used a zero-velocity reference layer at $\gamma^n = 27.38$ kg/m^3 (roughly 700 m depth) in the LP (stations 1–10) and in the southern section over the African slope (stations 45–51), and at $\gamma^n = 27.975$ kg/m^3 (roughly 1700 m depth) in the remaining stations. This layer of no motion in the LP has been used in previous studies (Hernández-Guerra et al., 2001, 2005; Pérez-Hernández et al., 2013). The layer of no motion at $\gamma^n = 27.975$ kg/m^3 is located in the deep layers with an approximately flat isoneutral slope. Comas-Rodriguez et al. (2011) noticed that the adjusted geostrophic transport to LADCP data has a zero velocity and an opposite velocity direction at this neutral density. Near the African shelf, where the deepest common depth is shallower than the reference level, the bottom is considered as the reference layer. Below the deepest common level of each station pair, velocities are considered to be constant.

Comas-Rodríguez et al. (2010) describe the procedure used to adjust the initial geostrophic velocity to LADCP-derived velocities from the two adjacent stations. A possible complication of using LADCP data is that velocities may not be geostrophically balanced, especially near the surface. Therefore, the first surface meters of the ocean have not been chosen for the velocity field comparison. A depth interval over which the vertical structures of LADCP velocities were similar to the geostrophic velocity profile is used to estimate the geostrophic reference velocity

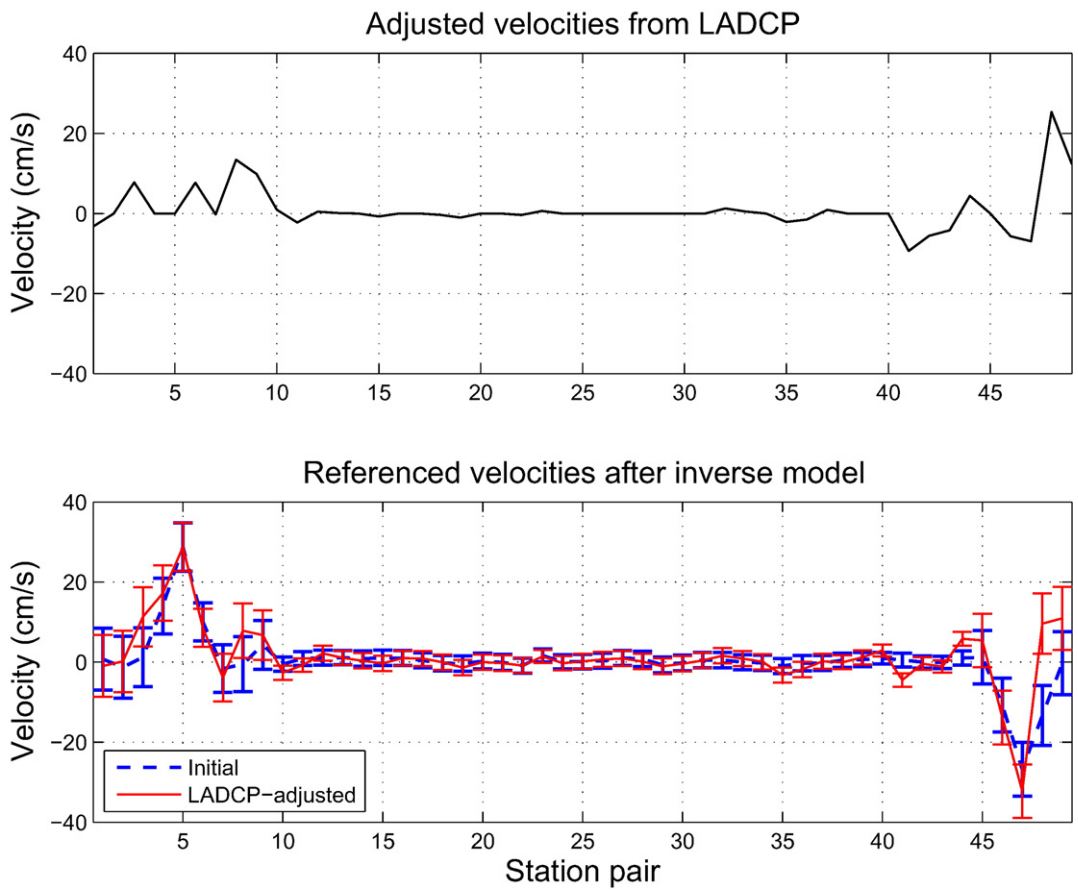

Fig. 9. a) Adjusted velocities matching the geostrophic velocity profile with the LADCP velocity profiles; b) Velocity determined by the inverse model using mass conservation (blue line) and velocity determined by the inverse model using LADCP adjusted velocities (red line). The sign of the velocity is geographic.

for each station pair. This procedure has been applied to the entire cruise. We specifically want to point out the results of the LP and to the southern section over the African slope due to the opposite initial flow in both transects.

Fig. 7 shows four profiles of LADCP-derived velocity and geostrophic velocity in the LP and southern section over the African slope. The oscillatory behavior of the LADCP profiles are probably due to the high frequency, ageostrophic movements. However, the shapes of the geostrophic velocity are similar to the LADCP velocity shapes. After a visual inspection of the profiles, we select a depth interval to match the geostrophic velocity profile with the LADCP profiles. The reference velocities are usually positive although they can also be negative as in station pair 48–49 (Fig. 7c) but these are much smaller than the positive velocities. Thus, the adjusted velocities provide the northward flow through the LP at a rate of 1.4 Sv in the thermocline layers and also in the southern transect over the African slope with a mass transport of 2.8 Sv.

5. Relative geostrophic transport

We have previously described how to infer the velocity at the reference layer using the geostrophic velocity profiles and LADCP velocity. Thus, two integrated mass transports per isoneutral are computed, the initial and the LADCP-adjusted geostrophic mass transports (Fig. 8). Both transports present a certain imbalance: −6.7 Sv for the initial transport and 6.6 Sv for the LADCP-adjusted transport. The structure of the imbalance changes when the LADCP-adjusted velocities are used. The initial mass transport imbalance mainly occurs in the surface and thermocline layers (layers 1 to 4). In contrast, the imbalance in these layers reduces in the LADCP-adjusted mass transport and increases in the intermediate and deep layers with opposite divergence.

6. Inverse model

As seen in Fig. 8, the mass transport presents a certain imbalance (about 6 Sv). Thus, an inverse model is applied in order to estimate the velocities at the reference layer that conserve mass transport. The inverse model was firstly introduced by Wunsch (1977) and has been extensively applied in different oceanographic areas (for further information see Wunsch (1996)). Ekman transport is also adjusted in our inverse model as in Ganachaud (2003) and Hernández-Guerra et al. (2014). An underestimated set of equations comprising the thermal wind equation and mass conservation composes the inverse method. The inverse box model assumes a time independence of the data. The cruise was carried out over 10 days which is presumably shorter than the time scale variability of the flow field in the ocean interior. In order to apply the inverse model, the closed ocean volume is divided into 13 layers by means of the neutral densities γ^n as previously carried out in the Canary Islands area (Hernández-Guerra et al., 2005; Pérez-Hernández et al., 2013). The inverse box model takes into account mass conservation per layer and the total mass without considering diapycnal interchanging. Ekman transport has been added to the shallowest layer. Thus, the inverse model solves the following equation:

$$\iint \rho b \; dx \; dz = -\iint \rho v_r \; dx \; dz - T_E \tag{1}$$

where ρ is the density of the ocean, b are the velocities at the reference layer at each station pair and the adjustment of the Ekman transport per

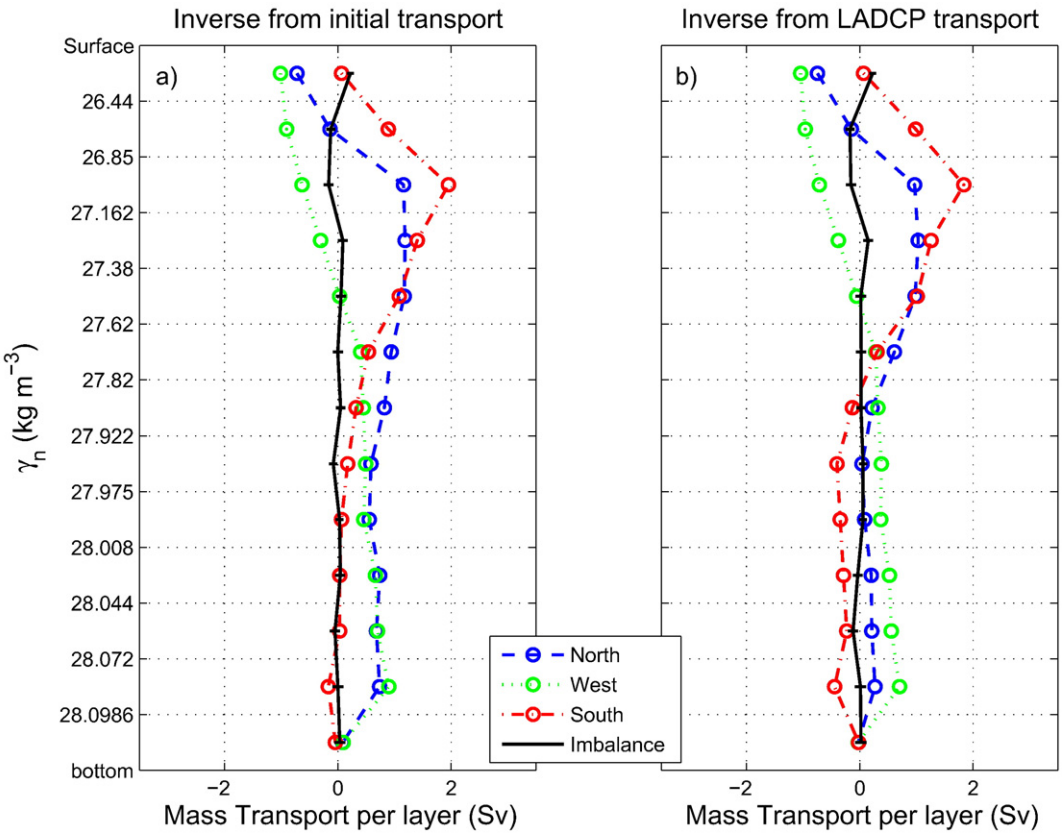

Fig. 10. Integrated final geostrophic mass transport per isoneutral layer, once applied the inverse model for the north (red), west (green) and south (blue) transects. Imbalance is represented by the black line with its uncertainty. a) Without LADCP adjusted velocities; b) with LADCP adjusted velocities. For each transect, positive/negative sign means northward/southward or eastward/westward flow.

section (the unknowns), x is the horizontal coordinate along the section, z is the vertical coordinate and T_E is the initial Ekman transport.

As we consider mass conservation equations for each layer and the total, the following matrix equation has to be solved:

$$\mathbf{A}\mathrm{x} + \mathrm{n} = -\mathrm{Y} \tag{2}$$

where **A** is a M × N matrix, where M is the number of transport constraints and N the number of the unknowns, ***n*** is a column vector whose elements are the noise of each equation, ***Y*** is a vector representing the mass transport initially imbalanced in each layer, and ***x*** is the column vector containing the unknown of the system:

$$\begin{pmatrix} (b_i)_{\mathrm{i}=1,\ldots,\mathrm{N_{pair}}} \\ \Delta T_E \end{pmatrix} \tag{3}$$

where b_i is the reference velocity in each station pair that adjust the mass transport, $\mathrm{N_{pair}}$ is the number of station pairs and ΔT_E is the adjustment of the Ekman transport.

In this study, the same inverse model has been applied to both the initial mass transport and the mass transport adjusted to the referenced velocities estimated from LADCP data. In both cases, the inverse model consists of 14 equations containing mass conservation per layer and total, and 52 unknowns, the velocities at the reference layer and the adjustment of the Ekman transport for each section. To solve this underestimated system of equations, the Gauss-Markov method which produces a minimum error variance solution from initial estimations of the unknowns is used. The preliminary variances of the reference-level velocity are $(8\ \mathrm{cm\ s^{-1}})^2$ for the station pairs located in the LP (stations 1–10) and over the African slope (stations 46–51) and $(2\ \mathrm{cm\ s^{-1}})^2$ for open ocean station pairs. A high preliminary variance is given to the LP and over the African slope as the LADCP presents very high velocities in these regions. The preliminary values of Ekman mass transport from wind data are −0.01 Sv, 0.01 Sv and 0.02 Sv through the north, west and south sections, respectively. Wind data during the time of the cruise present a very high variability and therefore their corresponding preliminary variances are kept high (90% of the initial Ekman transport). The inverse model do not change the initial values of Ekman transport in both models.

The preliminary uncertainties for the equations are $(0.1\ \mathrm{Sv})^2$ for each layer and $(1\ \mathrm{Sv})^2$ for overall mass transports. Gauss-Markov method provides a solution (the velocities at the reference layer per station pair) and an uncertainty of the solution. Thus, an uncertainty of the mass transport is also estimated.

7. Final geostrophic transport

Fig. 9 shows the adjusted velocities from LADCP (top plot) and the velocities in the referenced layer after the inverse model using the initial geostrophic mass transport and the transport adjusted to LADCP data (bottom plot). Fig. 9a shows that the velocities in the ocean interior adjusted to LADCP are very small, in the range of $\pm 1\ \mathrm{cm\ s^{-1}}$. Velocities are higher in the LP (station pairs 1–9) and in the southern transect over the African slope (station pairs 46–51). Velocities in the LP are predominantly positive (to the north) which will turn the initial southward transport in the passage to the north. In contrast, velocities in the African slope of the southern transect are mainly negatives that will decrease the initial northward transport. These high velocities as found from LADCP data are the cause for the high preliminary variance allowed in the inverse model in the LP and over the African slope of the southern transect.

Fig. 9b shows that the velocities in the reference layer after the inverse model has been applied have similar structure for both solutions.

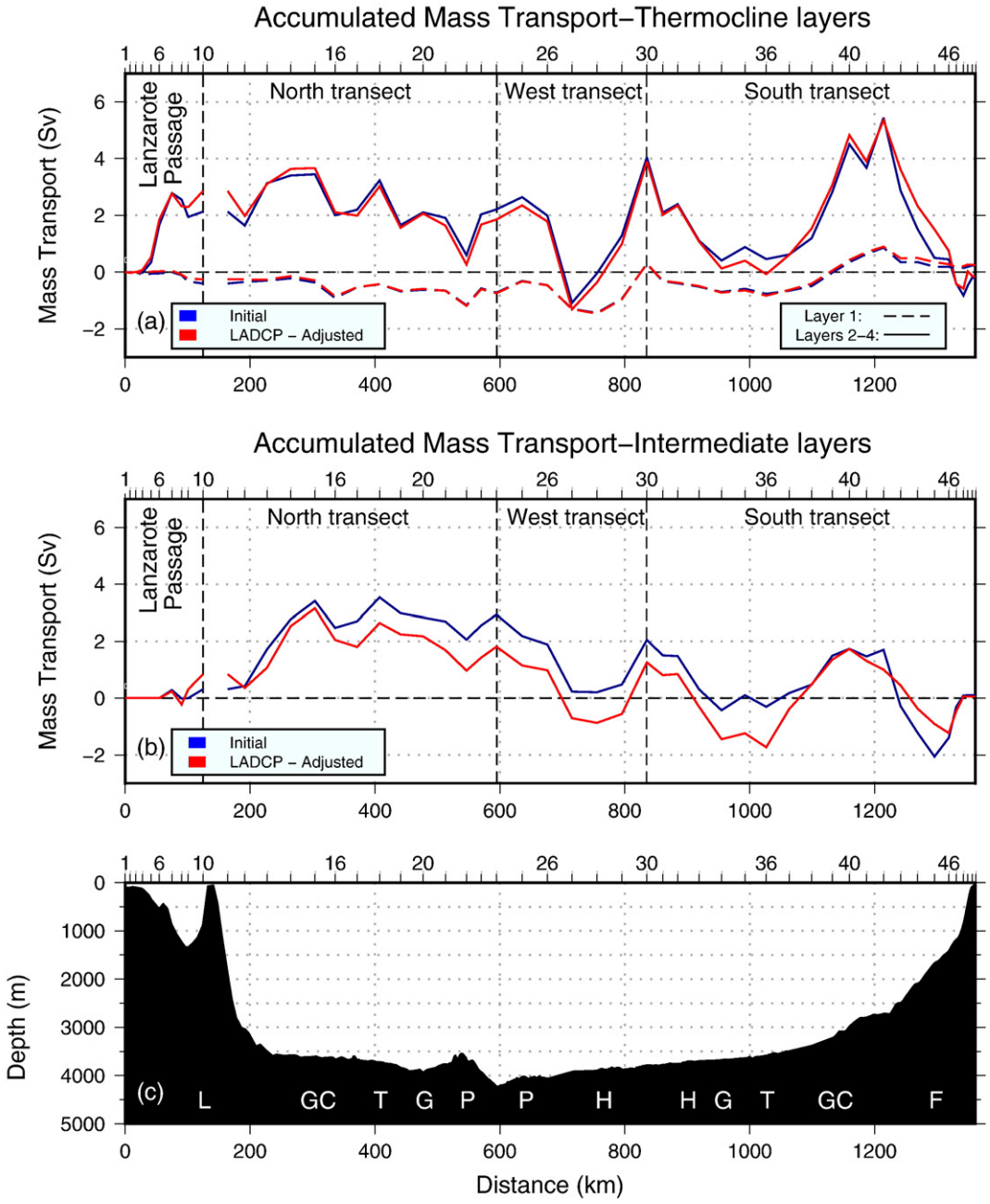

Fig. 11. Integrated mass transport for different group of layers after the inverse model with initial mass transport (blue line) and velocities adjusted to LADCP velocity data (red data): a) surface and thermocline layers (layer 1, dashed line; layers 2–4, solid line, $\gamma^n < 27.38$), and b) intermediate layers (layers 5–6, $27.38 < \gamma^n < 27.82$) as result of the inverse model. The integration starts in the northern section at the coast of Africa. The gap in the integrated mass transport in figures a) and b) is at Lanzarote island. Ticks on the top axis indicate the location of the stations. C) Labeled bathymetry for reference. L stands for Lanzarote, GC for Gran Canaria, T for Tenerife, G for La Gomera, P for La Palma, H for El Hierro.

They are small and not significantly different than zero in the ocean interior while they become higher in the LP and over the southern transect African slope. This modifies the adjusted velocities although the pattern is not changed: The velocities in the layer of reference have different directions resulting in an increase and decrease of the northward flow in the LP and in the African slope of the southern transect, respectively.

Fig. 10 shows the integrated final geostrophic mass transport per isoneutral layer obtained as result of inverse models. As already mentioned, it has been estimated without and with LADCP-adjusted velocity. Comparing both results, the mass transport shows a very similar pattern for each transect and the model estimations adjust the imbalance being now indistinguishable from zero: the total imbalance in mass transport is 0.1 ± 0.7 Sv and 0.3 ± 0.7 Sv without and with LADCP-adjusted data, respectively.

Results from the inverse model not using the LADCP adjusted velocities will be referred as initial inverse. When results for both inverse models are indistinguishable taking into account their uncertainty, the LADCP-adjusted mass transport only will be indicated. Fig. 11 shows the integrated mass transport for different groups of layers corresponding to the thermocline shallowest layer (layer 1), thermocline layers (layers 2–4) and intermediate layers (layers 5–6).

In the LP, the shallowest layer presents a southward flow of -0.3 ± 0.1 Sv for both solutions. The thermocline layers (2–4) show a northward transport of 2.1 ± 0.5 Sv in the initial inverse model solution and 2.9 ± 0.5 Sv in the LADCP-adjusted inverse model solution (Fig.

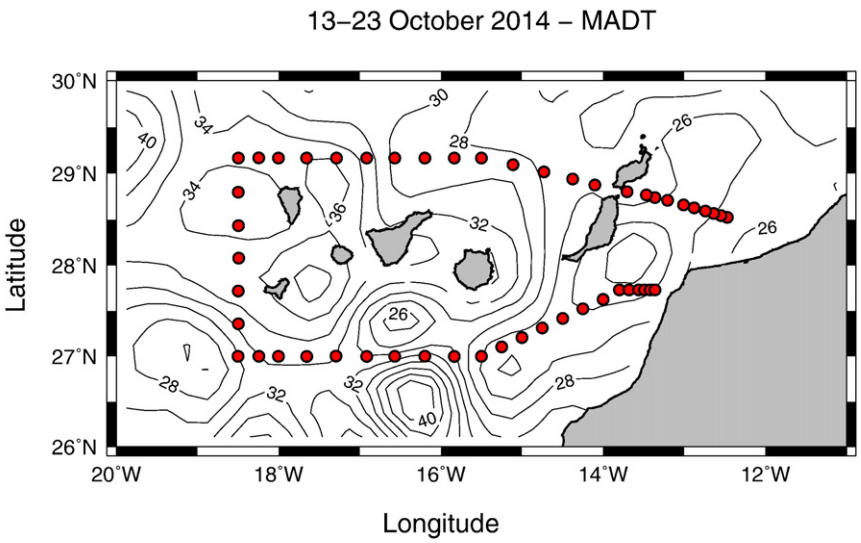

Fig. 12. Map of Absolute Dynamic Topography (MADT) as obtained from a mean (13–23 October 2014) of merged altimeter data. The points indicate the hydrographic stations.

11a). Both results are not significantly different due to their uncertainties. Northward currents in the LP have been observed previously in autumn with a mooring consisting of five current-meters deployed in the passage (Fraile-Nuez et al., 2010; Hernández-Guerra et al., 2003; Pérez-Hernández et al., 2015). A previous classical inverse model carried out by Hernández-Guerra et al. (2005) has also provided of a northward, although weaker transport in the LP of 1.1 ± 0.5 Sv.

Southward flow starts west of the Lanzarote island, defining the CC comprising layers 1 to 4. This southward mass transport is not significantly different than zero (−0.2 ± 0.7 Sv) in the classical inverse model and −1.5 ± 0.7 Sv in the LADCP adjusted model estimations. In contrast, Machín et al. (2006) describe a Canary Current that flows close to the Lanzarote island with a mass transport of −2.7 ± 0.4 Sv to the south.

In the western transect, there are two relatively large mesoscale eddies, with a radius of approximately 120 km. An anticyclonic eddy localized in the central part of the section with a rotating transport of 3.9 ± 0.4 Sv and a cyclonic eddy in the southwestern corner of our survey with a rotating transport of 4.2 ± 0.3 Sv. The existence of the southwestern eddy hinders the transport estimation in the western section. The

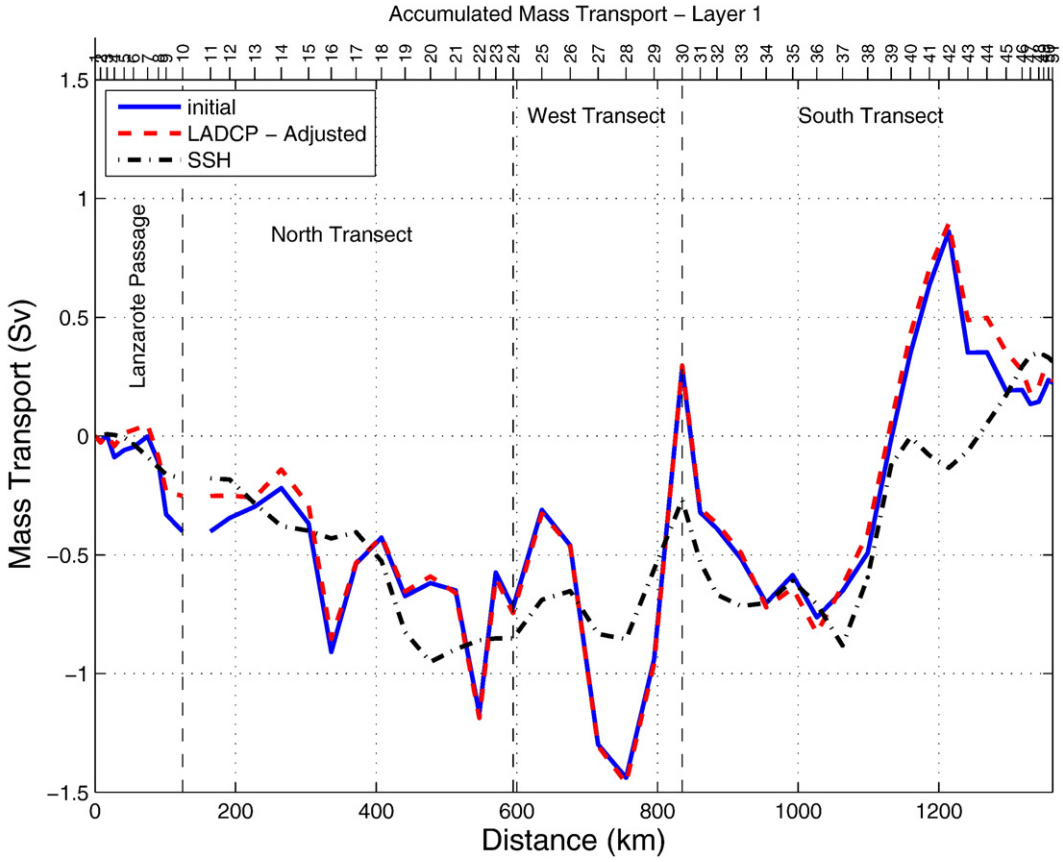

Fig. 13. Accumulated mass transport for layer 1 (initial and LADCP-adjusted) as result of the inverse model and accumulated mass transport estimated from Sea Surface Height (SSH) from altimetry for the whole cruise.

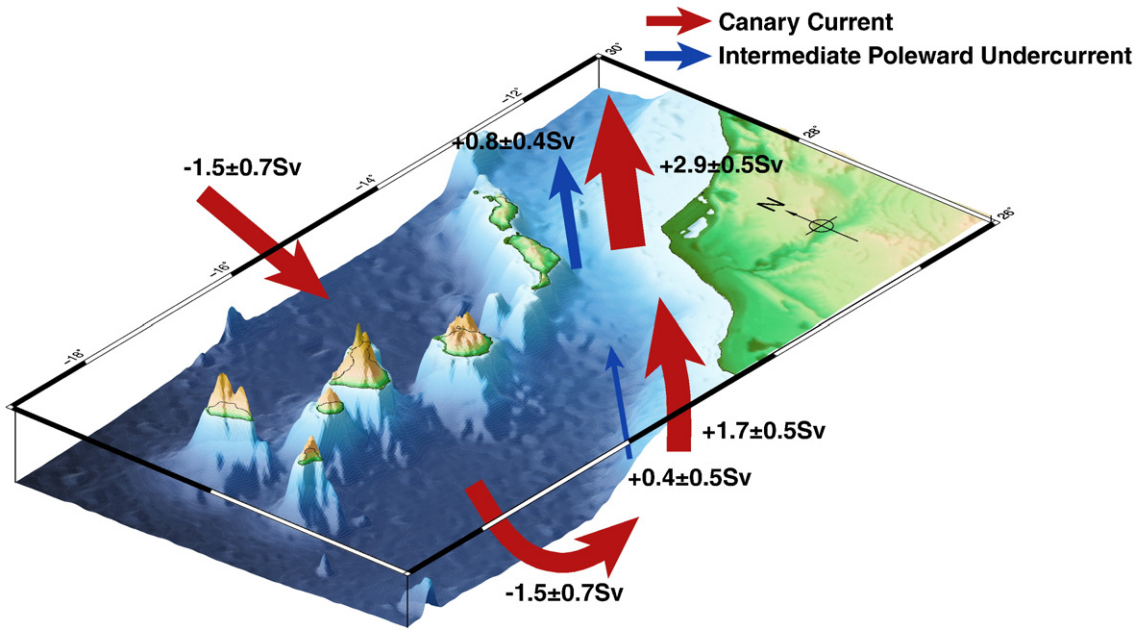

Fig. 14. Schematic diagram of the Canary Current (CC) and the Intermediate Poleward UnderCurrent (IPUC) in fall 2014. Red arrows stand for the CC flowing at thermocline layers and its recirculation and blue arrows stand for the IPUC. Estimated mass transport from inverse model for each arrow are shown. The North is indicated by way of the wind rose. The arrow width is proportional to the current.

net mass transport seen in Fig. 11a in the boundary between the western and the southern transect is presumably due to the cyclonic eddy and therefore the net mass transport in the western section is indistinguishable of zero. The integrated mass transport at the southern section also contains two adjacent eddies: an anticyclonic eddy and a cyclonic eddy whose rotating transports are 2.6 ± 0.3 Sv and 5.1 ± 0.3 Sv with radii of 180 and 250 km, respectively. These mesoscale eddies in the western and southern sections are generated downstream of the islands as a result of a Von Karman street phenomena (Hernández-Guerra et al., 1993; Pacheco and Hernández-Guerra, 1999; Sangra et al., 2007). As seen in Fig. 11a, the eddies located in the western and southern sections are more energetic than the eddies found in the northern section. The presence of the Canary Islands perturbs both the atmospheric and the oceanic flow. With this eddy signal it is complicated to estimate the path of the CC south of the islands that matches the −1.5 ± 0.7 Sv transported through the northern section. The signal of the CC is presumably embedded within the signal of the eddies.

In the eastern boundary of the southern section (from station 45 to the African shelf), the inverse model solution shows a non-significant transport in the first layer (0.1 ± 0.2 Sv) and a northward transport of 0.7 ± 0.5 Sv from the classical inverse model and 1.7 ± 0.5 Sv from the LADCP-adjusted model (Fig. 11a). This northward transport matches the transport through the LP.

Fig. 12 shows the Map of Absolute Dynamic Topography (MADT) for the time of the cruise. This map roughly resembles the mass transport of the first layer (Fig. 11a): A southward transport in the northern section and energetic eddies in the western and southern sections are clearly visible in the Sea Surface Height (SSH) (Fig. 12). In order to check the relationship between the SSH from altimetry and the mass transport from hydrographic data, Fig. 13 compares the accumulated mass transport for the first layer with the estimated from altimetry following the procedure described in Vélez-Belchí et al. (2013). The correlation coefficient between both data is 0.81 resulting in a high and positive correlation between them.

Fig. 11b shows integrated the mass transport for the intermediate layers (layers 5–6). The mass transport through the LP is 0.8 ± 0.4 Sv to the north for the LADCP-adjusted solution and not significantly different than zero for the initial solution (0.3 ± 0.4 Sv). The eastern boundary at the southern section (stations 43 to 51) presents a non-significant northward transport for both inverse model solutions (0.4 ± 0.5 Sv). The current associated with this northward transport is called IPUC carrying AAIW to the passage (see Fig. 4).

8. Discussion and conclusions

The ocean circulation in the Canary Basin from a cruise carried out in October 2014 has been inferred. The initial geostrophic mass transport has been estimated with and without LADCP data as an estimate for the velocity at the reference level. An inverse box model has also been applied in both initial mass transports to estimate new velocities at the reference level that conserve mass. Both solutions converge giving confidence of the inverse model.

Fig. 14 summarizes the estimated circulation in the Canary Basin in fall 2014. The CC flows to the south in the thermocline layers (0–700 m) transporting NACW at a rate of −1.5 ± 0.7 Sv west of Lanzarote Island. The classical inverse model describes a CC that is not significantly different than zero as in previous results that apply initial inverse models to hydrographic data collected in fall (Pérez-Hernández et al., 2013). This result emphasizes the use of LADCP data to estimate a velocity in the reference layer before the inverse estimations (Joyce et al., 2001). The exact path of the CC is difficult to infer due to existing mesoscale features in the northern section and longer eddies shed by the islands in the western and southern sections. These cyclonic and anticyclonic eddies located downstream of the islands have been extensively studied as result of a mass island effect (Arístegui et al., 1994; Sangra et al., 2005, 2009). Their clock/counterclockwise transport doubles the transport of the CC.

The isoneutrals in the thermocline layers through the LP and over the African slope present opposite inclination resulting in a geostrophic shear flow convergence. The adjustment of the geostrophic velocity profile to the LADCP velocity profiles provides the northward circulation across the LP and over the African slope at 27°N except in layer 1. The northward mass transport over the African slope is 1.7 ± 0.5 Sv at 27°N increasing to 2.9 ± 0.5 Sv through the LP. Thus, the southward CC recirculates to the north over the African slope and through the LP as inferred from hydrographic data. In the maps of dynamic height from altimetry data presented by Pérez-Hernández et al. (2015), the northward flow through the LP is apparently a northward branch of

the CC. They also suggested that the large eddies shed from the islands observed in the southern section can reinforce the cyclonic circulation south of the Canary Islands as also observed in Mason et al. (2011), leading to the recirculation of the CC. It has been speculated that the CUC is due to the upwelling dynamics off northwest Africa: An upwelling front results in an upwelling jet that originates the CUC. The northward flow through the LP in fall is a recirculation of the CC with apparently no link to the upwelling dynamics as suggested by Mason et al. (2011). The CUC would be the southward transport of -0.3 ± 0.1 Sv in the shallowest layer.

At intermediate layers, warmer and saltier MW and fresher AAIW are found at 29°N and 27°N, respectively. The LP is the only location where a higher content of AAIW is measured at 29°N as originally described in Hernández-Guerra et al. (2001). On this occasion, relatively fresh water corresponding to AAIW is also observed west of Lanzarote island resulting that the northward flow of the IPUC is broader than the LP. Low salinity waters just west of Lanzarote Island are also seen in Pérez-Hernández et al. (2013). Machín and Pelegrí (2009) were the first to demonstrate that intense Ekman pumping localized near the tropical African coast elevates the upper isoneutrals, stretching the intermediate water column. Due to conservation of potential vorticity, this results in a northward flow along the African slope (Machín et al., 2010).

In conclusion, fall 2014 provides the first evidence, from in situ observations, of a recirculation of the CC through the LP and of an IPUC that flows northward at intermediate layers extending to the west of Lanzarote Island.

Acknowledgments

This study has been performed as part of the Instituto Español de Oceanografía RAPROCAN project, and as a part of the SeVaCan project (CTM2013–48695) from the Ministerio de Economía y Competividad. This work was completed while M.D. Pérez-Hernández was a Ph.D. student in the IOCAG Doctoral Programme in Oceanography and Global Change. The authors are grateful to the captain and crew of the R/V Ángeles Alvariño for their help at sea. Many thanks go to David Sosa and Rayco Alvarado for helping with data treatment and figures and Christina Mock for her suggestions and English corrections.

References

Arístegui, J., Sangra, P., Hernandez-Leon, S., Canton, M., Hernández-Guerra, A., Kerling, J.L., 1994. Island-induced eddies in the Canary-Islands. Deep-Sea Res. Pt. I 41, 1509–1525.

Benazzouz, A., Mordane, S., Orbi, A., Chagdali, M., Hilmi, K., Atillah, A., Pelegrí, J.L., Demarcq, Hervé, 2014. An improved coastal upwelling index from sea surface temperature using satellite-based approach – the case of the Canary Current upwelling system. Cont. Shelf Res. 81:38–54. http://dx.doi.org/10.1016/j.csr.2014.03.012.

Borges, R., Hernández-Guerra, A., Nykjaer, L., 2004. Analysis of sea surface temperature time series of the south-eastern North Atlantic. Int. J. Remote Sens. 25:869–891. http://dx.doi.org/10.1080/0143116031000082442.

Comas-Rodríguez, I., Hernández-Guerra, A., McDonagh, E.L., 2010. Referencing geostrophic velocities using ADCP data at 24.5°N (North Atlantic). Sci. Mar. 74:331–338. http://dx.doi.org/10.3989/scimar.2010.74n2331.

Comas-Rodriguez, I., Hernández-Guerra, A., Fraile-Nuez, E., Martínez-Marrero, A., Benítez-Barrios, V.M., Perez-Hernandez, M.D., Vélez-Belchí, P., 2011. The Azores Current System from a meridional section at 24.5°W. J. Geophys. Res-Oceans. 116:C09021. http://dx.doi.org/10.1029/2011JC007129.

Firing, E., Ranada, E., 1995. Processing ADCP Data With the CODAS Software System. Joint Institute for Marine and Atmospheric Research.

Fischer, J., Visbeck, M., 1993. Deep velocity profiling with self-contained ADCPs. J. Atmos. Ocean. Technol. 10, 764–773.

Fraile-Nuez, E., Hernández-Guerra, A., 2006. Wind-driven circulation for the eastern North Atlantic subtropical gyre from Argo data. Geophys. Res. Lett. 33. http://dx.doi.org/10.1029/2005GL025122.

Fraile-Nuez, E., Machín, F., Vélez-Belchí, P., López-Laatzen, F., Borges, R., Benítez-Barrios, V., Hernández-Guerra, A., 2010. Nine years of mass transport data in the eastern boundary of the North Atlantic subtropical gyre. J. Geophys. Res-Oceans. 115. http://dx.doi.org/10.1029/2010JC006161.

Ganachaud, A., 1999. Global Oceanic Circulation and Fluxes of Freshwater, Heat, Nutrients and Oxygen (Ph.D. Thesis. MIT and WHOI joint program, 266 pp.).

Ganachaud, A., 2003. Large-scale mass transports, water mass formation, and diffusivities estimated from World Ocean Circulation Experiment (WOCE) hydrographic data. J. Geophys. Res. 108:3213. http://dx.doi.org/10.1029/2002JC001565.

Hernández-Guerra, A., Nykjaer, L., 1997. Sea surface temperature variability off northwest Africa: 1981–1989. Int. J. Remote Sens. 18, 2539–2558.

Hernández-Guerra, A., Talley, L.D., 2016. Meridional overturning transports at 30°S in the Indian and Pacific Oceans in 2002–2003 and 2009. Prog. Oceanogr. 146:89–120. http://dx.doi.org/10.1016/j.pocean.2016.06.005.

Hernández-Guerra, A., Arístegui, J., Canton, M., Nykjaer, L., 1993. Phytoplankton pigment patterns in the Canary Islands area as determined using Coastal Zone Colour Scanner data. Int. J. Remote Sens. 14, 1431–1437.

Hernández-Guerra, A., López-Laatzen, F., Machín, F., De Armas, D., Pelegri, J., 2001. Water masses, circulation and transport in the eastern boundary current of the North Atlantic subtropical gyre. Sci. Mar. 65 (Suppl. 1), 177–186.

Hernández-Guerra, A., Machın, F., Antoranz, A., Cisneros-Aguirre, J., Gordo, C., Sangra, P., Marrero-Diaz, A., Martinez, A., Ratsimandresey, A., Rodriguez-Santana, A., Sangra, P., 2002. Temporal variability of mass transport in the Canary Current. Deep-Sea Res. II Top. Stud. Oceanogr. 49, 3415–3426.

Hernández-Guerra, A., Fraile-Nuez, E., Borges, R., López-Laatzen, F., Vélez-Belchí, P., Parrilla, G., Muller, T., 2003. Transport variability in the Lanzarote passage (eastern boundary current of the North Atlantic subtropical gyre). Deep-Sea Res. Pt. I 50: 189–200. http://dx.doi.org/10.1016/S0967-0637(02)00163-2.

Hernández-Guerra, A., Fraile-Nuez, E., López-Laatzen, F., Martínez, A., Parrilla, G., Vélez-Belchí, P., 2005. Canary Current and North Equatorial Current from an inverse box model. J. Geophys. Res. 110. http://dx.doi.org/10.1029/2005JC003032.

Hernández-Guerra, A., Pelegrí, J.L., Fraile-Nuez, E., Benítez-Barrios, V.M., Emelianov, M., Pérez-Hernández, M.D., Vélez-Belchí, P., 2014. Meridional overturning transports at 7.5N and 24.5N in the Atlantic Ocean during 1992–93 and 2010–11. Prog. Oceanogr. 128:98–114. http://dx.doi.org/10.1016/j.pocean.2014.08.016.

Jackett, D.R., McDougall, T.J., 1997. A neutral density variable for the world's oceans. J. Phys. Oceanogr. 27, 237–263.

Joyce, T., Hernández-Guerra, A., Smethie, W., 2001. Zonal circulation in the NW Atlantic and Caribbean from a meridional World Ocean Circulation Experiment hydrographic section at 66 degrees W. J. Geophys. Res-Oceans. 106, 22095–22113.

Knoll, M., Hernández-Guerra, A., Lenz, B., López-Laatzen, F., Machın, F., Muller, T.J., Siedler, G., 2002. The eastern boundary current system between the Canary Islands and the African coast. Deep-Sea Res. II Top. Stud. Oceanogr. 49, 3427–3440.

Laiz, I., Pelegrí, J.L., Machín, F., Sangra, P., Hernández-Guerra, A., Marrero-Diaz, A., Rodríguez-Santana, A., 2012. Eastern boundary drainage of the North Atlantic subtropical gyre. Ocean Dyn. 62, 1287–1310.

Machín, F., Pelegrí, J.L., 2009. Northward penetration of Antarctic intermediate water off Northwest Africa. J. Phys. Oceanogr. 39, 512–535.

Machín, F., Hernández-Guerra, A., Pelegrí, J.L., 2006. Mass fluxes in the Canary Basin. Prog. Oceanogr. 70:416–447. http://dx.doi.org/10.1016/j.pocean.2006.03.019.

Machín, F., Pelegrí, J.L., Fraile-Nuez, E., Vélez-Belchí, P., López-Laatzen, F., Hernández-Guerra, A., 2010. Seasonal flow reversals of intermediate waters in the Canary Current system east of the Canary Islands. J. Phys. Oceanogr. 40, 1902–1909.

Marcello, J., Hernández-Guerra, A., Eugenio, F., Fonte, A., 2011. Seasonal and temporal study of the northwest African upwelling system. Int. J. Remote Sens. 32: 1843–1859. http://dx.doi.org/10.1080/01431161003631576.

Mason, E., Colas, F., Molemaker, J., Shchepetkin, A.F., Troupin, C., McWilliams, J.C., Sangra, P., 2011. Seasonal variability of the Canary Current: a numerical study. J. Geophys. Res-Oceans. 116. http://dx.doi.org/10.1029/2010JC006665.

Mason, E., Colas, F., Pelegrí, J.L., 2012. A Lagrangian study tracing water parcel origins in the Canary Upwelling System. Sci. Mar. 76:79–94. http://dx.doi.org/10.3989/scimar.03608.18D.

Nykjaer, L., Van Camp, L., 1994. Seasonal and interannual variability of coastal upwelling along northwest Africa and Portugal from 1981 to 1991. J. Geophys. Res. 99, 14197–14207.

Pacheco, M.M., Hernández-Guerra, A., 1999. Seasonal variability of recurrent phytoplankton pigment patterns in the Canary Islands area. Int. J. Remote Sens. 20, 1405–1418.

Parrilla, G., 2002. Topical studies in oceanography: Canary Islands Azores Gibraltar Observations (CANIGO). Volume 1: studies in the northern Canary Islands basin. Deep-Sea Res. II 49, 3409–3413.

Pelegrí, J.L., Arístegui, J., Cana, L., Gonzalez-Davila, M., Hernández-Guerra, A., Hernandez-Leon, S., Marrero-Diaz, A., Montero, M.F., Sangra, P., Santana-Casiano, M., 2005. Coupling between the open ocean and the coastal upwelling region off northwest Africa: water recirculation and offshore pumping of organic matter. J. Mar. Syst. 54:3–37. http://dx.doi.org/10.1016/j.jmarsys.2004.07.003.

Pelegrí, J.L., Marrero-Diaz, A., Ratsimandresey, A.W., 2006. Nutrient irrigation of the North Atlantic. Prog. Oceanogr. 70:366–406. http://dx.doi.org/10.1016/j.pocean.2006.03.018.

Pérez-Hernández, M.D., Hernández-Guerra, A., Fraile-Nuez, E., Comas-Rodríguez, I., Benítez-Barrios, V.M., Domínguez-Yanes, J.F., Vélez-Belchí, P., Armas, D., 2013. The source of the Canary current in fall 2009. J. Geophys. Res-Oceans. 118:2874–2891. http://dx.doi.org/10.1002/jgrc.20227.

Pérez-Hernández, M.D., McCarthy, G.D., Vélez-Belchí, P., Smeed, D.A., Fraile-Nuez, E., Hernández-Guerra, A., 2015. The Canary Basin contribution to the seasonal cycle of the Atlantic Meridional Overturning Circulation at 26°N. J. Geophys. Res-Oceans. 120:7237–7252. http://dx.doi.org/10.1002/2015JC010969.

Roemmich, D., Wunsch, C., 1985. Two transatlantic sections: meridional circulation and heat flux in the subtropical North Atlantic Ocean. Deep-Sea Res. 32, 619–664.

Sangra, P., Pelegrí, J.L., Hernández-Guerra, A., Arregui, I., Martin, J.M., Marrero-Díaz, Á., Martínez, A., Ratsimandresey, A.W., Rodríguez-Santana, Á., 2005. Life history of an anticyclonic eddy. J. Geophys. Res. 110 (C03021–19). 10.1029/2004JC002526.

Sangra, P., Auladell, M., Marrero-Diaz, A., Pelegrí, J.L., Fraile-Nuez, E., Rodríguez-Santana, A., Martin, J.M., Mason, E., Hernández-Guerra, A., 2007. On the nature of oceanic eddies shed by the Island of Gran Canaria. Deep-Sea Res. Pt. I 54:687–709. http://dx.doi.org/10.1016/j.dsr.2007.02.004.

Sangra, P., Pascual, A., Rodríguez-Santana, Á., Machín, F., Mason, E., McWilliams, J.C., Pelegrí, J.L., Dong, C., Rubio, A., Arístegui, J., Marrero-Díaz, Á., Hernández-Guerra, A., Martínez-Marrero, A., Auladell, M., 2009. The Canary Eddy Corridor: a major pathway for long-lived eddies in the subtropical North Atlantic. Deep-Sea Res. Pt. I 56: 2100–2114. http://dx.doi.org/10.1016/j.dsr.2009.08.008.

Skamarock, W.C., Klemp, J.B., Dudhia, J., Gill, D.O., Barker, D.M., Duda, M.G., Huang, X.-Y., Wang, W., Powers, J.G., 2008. A Description of the Advanced Research WRF Version 3 (No. NCAR/TN-475+STR), NCAR Technical Note.

Smith, W.H.F., 1997. Global Sea Floor topography from satellite altimetry and ship depth soundings. Science 277:1956–1962. http://dx.doi.org/10.1126/science.277.5334.1956.

Stramma, L., 1984. Geostrophic transport in the warm water sphere of the eastern subtropical North Atlantic. J. Mar. Res. 42, 537–558.

Stramma, L., Isemer, H.J., 1988. Seasonal variability of meridional temperature fluxes in the eastern North Atlantic Ocean. J. Mar. Res. 46:281–299. http://dx.doi.org/10.1357/002224088785113577.

Stramma, L., Müller, T.J., 1989. Some observations of the Azores Current and the North Equatorial Current. J. Geophys. Res. Ocean 94:3181–3186 (1978–2012). 10.1029/JC094iC03p03181.

Stramma, L., Siedler, G., 1988. Seasonal changes in the North Atlantic subtropical gyre. J. Geophys. Res. 93, 8111–8118.

Tel, E., Balbin, R., Cabanas, J.-M., Garcia, M.-J., Garcia-Martinez, M.C., Gonzalez-Pola, C., Lavín, A., Lopez-Jurado, J.-L., Rodriguez, C., Ruiz-Villarreal, M., Sánchez-Leal, R.F., Vargas-Yáñez, M., Vélez-Belchí, P., 2016. IEOOS: the Spanish Institute of Oceanography Observing System. Ocean Sci. 12:345–353. http://dx.doi.org/10.5194/os-12-345-201.

Van Camp, L., Nykjaer, L., Mittelstaedt, E., Schlittenhardt, P., 1991. Upwelling and boundary circulation off Northwest Africa as depicted by infrared and visible satellite observations. Prog. Oceanogr. 26, 357–402.

Vélez-Belchí, P., Centurioni, L.R., Lee, D.K., Jan, S., Niiler, P.P., 2013. Eddy induced Kuroshio intrusions onto the continental shelf of the East China Sea. J. Mar. Syst. 71:83–107. http://dx.doi.org/10.1357/002224013807343470.

Wooster, W.S., Bakun, A., McLain, D.R., 1976. Seasonal upwelling cycle along the eastern boundary of the North Atlantic. J. Mar. Res. 34, 131–141.

Wunsch, C., 1977. Determining the general circulation of the oceans: a preliminary discussion. Science 196, 871–875.

Wunsch, C., 1996. The Ocean Circulation Inverse Problem. Cambridge University Press.